Nuclear viscosity of hot rotating ^{240}Cf

N. P. Shaw,[1] I. Diószegi,[1] I. Mazumdar,[1] A. Buda,[1] C. R. Morton,[1] J. Velkovska,[1] J. R. Beene,[2] D. W. Stracener,[2] R. L. Varner,[2] M. Thoennessen,[3] and P. Paul[4]

[1]*Department of Physics and Astronomy, State University of New York at Stony Brook, Stony Brook, New York 11794-3800*
[2]*Oak Ridge National Laboratory, Oak Ridge, Tennessee 37831*
[3]*National Superconducting Cyclotron Laboratory and Department of Physics and Astronomy, Michigan State University, East Lansing, Michigan 48824*
[4]*Brookhaven National Laboratory, Upton, New York 11973*

The absolute γ-ray/fission multiplicities from hot rotating ^{240}Cf, populated at seven bombarding energies using the reaction ^{32}S$+^{208}$Pb, are reported. Statistical model calculations including nuclear dissipation have been performed to extract the dependence of the nuclear viscosity on temperature and/or nuclear deformation. The extracted nuclear dissipation coefficient is found to be independent of temperature. Large dissipation during the saddle to scission path provides a good fit to the γ-ray spectra.

PACS number(s): 25.70.Jj, 25.70.Gh, 24.30.Cz

I. INTRODUCTION

Compelling evidence for nuclear dissipation slowing down the fission process in excited ^{224}Th has been obtained in studies of giant dipole resonance γ-ray spectra [1–4] as well as neutron multiplicities [5]. Recently [4] we presented a detailed reinvestigation of nuclear dissipation in the system ^{16}O$+^{208}$Pb. The new step was that measured *absolute* γ-ray/fission multiplicities along with existing experimental neutron multiplicities and evaporation residue cross sections were analyzed consistently within the framework of a modified statistical model. While in the case of hot rotating ^{224}Th formed in the ^{16}O$+^{208}$Pb reaction the presence of strong nuclear dissipation was confirmed, the exact dependence on either temperature or deformation could not be unambiguously ascertained. The reanalysis confirmed the earlier observation of a rapid increase of nuclear dissipation with bombarding energy. When this rapid increase is translated into a temperature dependence, it has been cited [6] as evidence that two-body interactions are the underlying mechanism of nuclear dissipation. However, when the effect of the vanishing fission barrier with increasing angular momentum and temperature dependent transient effects are taken into account [4], an equally good fit to the data is provided by a deformation-dependent dissipation. This latter explanation would suggest that one-body dissipation is responsible for the fission delay process [7].

Since increasing the bombarding energy in a heavy ion fusion-fission reaction simultaneously raises the temperature and the average angular momentum of the compound nucleus (CN), it is difficult to determine the dependence of nuclear dissipation on these quantities separately. In a very heavy, highly fissile CN the fission barrier vanishes at relatively low angular momenta. This leads to a new situation compared to ^{224}Th: the presaddle time (if it exists at all) becomes extremely short and the fission process is completely governed by transient effects. The complete mass and thermal equilibration takes place but the compound system arrives to the saddle point without any significant presaddle emission, or in case of vanishing fission barrier the system

itself is formed at the saddle point or the saddle point does not exist. At angular momenta higher than a critical value the quasifission process dominates, where the complete mass equilibration is not reached, the system starts its descent towards the scission point in a highly deformed configuration. With increasing bombarding energy the ratio of presaddle and saddle to scission γ-ray and neutron emission changes with increasing contribution coming from the saddle to scission path to the total yield.

Nuclear viscosity affects both the presaddle and saddle to scission motion. In ^{224}Th both pre- and post-saddle emission is present, therefore it was not possible to uniquely determine whether the increase in the measured dissipation with the bombarding energy arises from a temperature dependence of the viscosity, or the viscosity is larger outside the saddle, and this larger viscosity has increasingly higher contribution to the average viscosity at higher bombarding energies. To resolve this matter one should compare systems that are dominated by either presaddle or saddle to scission emission.

In the present work hot rotating ^{240}Cf has been chosen as a system in which the saddle to scission emission dominates the prescission particle and γ-ray spectra. Nuclear dissipation in ^{240}Cf was first studied by Hofman *et al.* [8] who reported a large nuclear viscosity parameter ($\gamma \sim 5$). That experiment was carried out at only two bombarding energies. Here we present data over a range of seven excitation energies. In addition, the present measurements provide absolute γ-ray/fission multiplicities thus removing any arbitrary normalization of the calculated spectra to the experimental data. This severely constrains the input model parameters and eliminates the uncertainties associated with the normalization method [4]. An analysis of the angular correlation data for the five lower bombarding energies of the present experiment has been published previously [9].

The organization of the present paper is as follows. The experimental details, the data reduction process, and the experimental results are presented in Sec. II. Section III reviews the basic ingredients of the model calculations. The

TABLE I. Summary of the reaction parameters for the ^{32}S+^{208}Pb→^{240}Cf reaction at different beam energies. The columns list the beam energy (E_{lab}), the total fusion cross section (σ_{tot}), the excitation energy of the system (E^*), the corresponding maximum (l_{max}) and average (l_{ave}) angular momenta, the Sierk fission barrier $\langle B_f \rangle$ at l_{ave}, and the initial temperature of the system (T) assuming $E^*=aT^2$ with $a=A/9$. The total fusion cross sections were obtained by extrapolating from the experimental fission cross section of Ref. [10].

E_{lab} (MeV)	σ_{tot} (mb)	E^* (MeV)	l_{max} ($\hbar$)	l_{ave} ($\hbar$)	$\langle B_f \rangle$ (MeV)	T (MeV)
180	155.0	45.5	31	21	1.2	1.3
200	428.2	63.0	54	36	0.6	1.5
215	660.3	76.0	81	54	0.0	1.7
230	828.3	89.9	91	61	0.0	1.8
245	952.7	103.0	99	67	0.0	2.0
265	1072.4	120.5	109	73	0.0	2.1
285	1161.2	138.0	116	78	0.0	2.3

data analysis is presented in Sec. IV followed by a discussion in Sec. V.

II. EXPERIMENTAL PROCEDURE AND RESULTS

A. Experimental setup

The experiment presented here was carried out using the Stony Brook Tandem-LINAC facility. A 870 μg/cm^2 thick self-supporting ^{208}Pb target mounted at 45° relative to the beam axis was bombarded with a pulsed ^{32}S beam at seven energies ranging from 180 MeV to 285 MeV. The relevant reaction parameters are summarized in Table I for each bombarding energy. The LINAC provided beams with an extremely stable time reference; the beam pulse repetition time was 106 ns with an average full width at half maximum of ≈800 ps.

High energy γ-rays were detected in coincidence with fission fragments in the large array of BaF$_2$ scintillation detectors from Oak Ridge National Laboratory, Michigan State University, Texas A&M University, and from Stony Brook. The array consists of 154 hexagonal crystals with dimensions ($d=6.5$ cm, $l=20$ cm) for 127 crystals, (6.0 cm, 20 cm) for 20 crystals and (5.6 cm, 14 cm) for the remaining seven crystals. Here d is the diameter of a circle that inscribes the front face of the crystal and l is the length of the crystal. The differences in dimensions were included in the determination of the array efficiency and response matrix. The array, installed in a close-packed wall configuration, was centered at $\theta_{lab}=90°$ at a distance of 54 cm from the target resulting in a total solid angle of 11% of 4π. A schematic diagram of the experimental setup is shown in Fig. 1. The high granularity of the system greatly reduced the probability of pileup events. The array was thermally isolated from its environment by an insulating shell and was temperature stabilized in order to reduce gain fluctuations due to the well known temperature dependence of BaF$_2$ light output. In addition, the array was frequently calibrated using a ^{88}Y source ($E_\gamma=0.898$ MeV and 1.836 MeV) during the course of the experiment. A 6 mm thick lead sheet shielded the front face and sides of the array from low energy γ-rays. Calibration points were also obtained with high energy γ-rays from pro-

ton induced reactions, ^{12}C$(p,\gamma)^{13}$N ($E_\gamma=15.1$ MeV) and ^{11}B$(p,\gamma)^{12}$C ($E_\gamma=18.12$ MeV and 22.56 MeV). The absolute efficiency of the array was obtained from an experimental comparison with a well characterized compact array of seven BaF$_2$ crystals [11]. A detailed investigation of efficiency using this small BaF$_2$ array has been described in Ref. [4].

Fission fragments were detected in four large multiwire avalanche counters (MWAC) positioned in a target chamber designed specifically for measurement of forward-focused fission fragments. The fission fragments were identified by energy loss (ΔE) and time-of-flight (TOF). A subset of the data consists of events where both fission fragments from a fused system are detected in kinematic coincidence. The detailed design, position calibration and performance of these detectors have been discussed elsewhere [3].

The dedicated electronics associated with this large BaF$_2$ array included CAMAC ADCs and FASTBUS TDCs for measurement of energy and TOF and a VME-controlled data acquisition system. The LINAC radio-frequency master clock provided the timing reference for the electronics. The
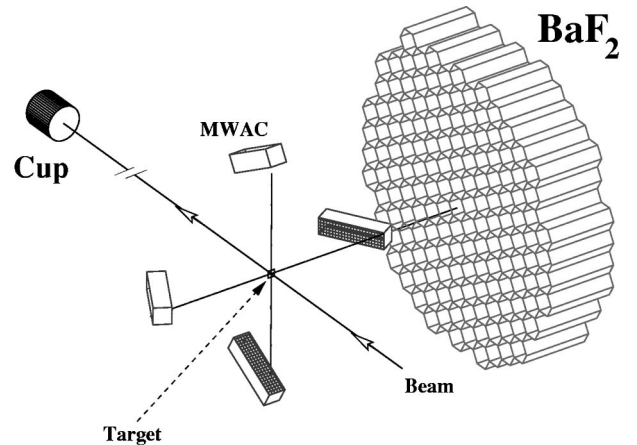
FIG. 1. Schematic diagram of the experimental setup with the 154 element BaF$_2$ array in the wall configuration centered at $\theta_{lab}=90°$ with respect to the beam axis and the four MWACs arranged for detection of forward focused fission fragments.
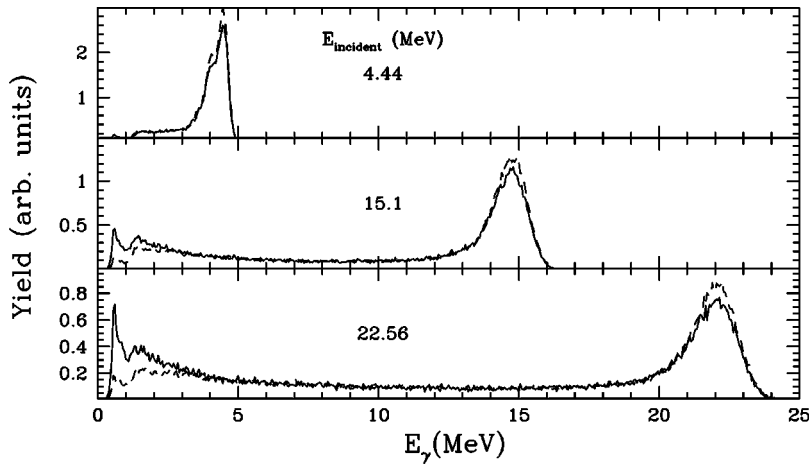
FIG. 2. Comparison of simulated energy spectra for monoenergetic γ rays at three energies reconstructed using the strict contiguity algorithm (solid lines) and the more relaxed contiguity condition (dashed lines).

main event trigger required at least one BaF$_2$ detector with an energy deposition greater than a high threshold T_h ≈ 3 MeV. This trigger condition also required an event in at least one MWAC. If the high threshold T_h condition was satisfied, energy and TOF spectra were recorded for all detectors with energy deposition greater than a low threshold $T_l \approx 300$ keV. Separate 50 ns and 1500 ns gates were used to integrate the fast component and total (slow) yield of the BaF$_2$ light output, respectively, for use in the fast versus slow pulse-shape analysis for pileup rejection. A different downscaled event trigger type required only single MWAC events and was used for determination of the γ-ray/fission multiplicities. A detailed discussion of the electronics and trigger handling is presented in Ref. [12].

B. Data reduction process

The extraction of final spectra from a large multielement array is an involved process requiring accurate event reconstruction and determination of the array response. A high-energy particle or γ-ray impinging upon an element in the array will deposit its energy in an electromagnetic shower which often extends laterally beyond more than one element. Reconstructing the incident energy of the particle requires summing the energy from all elements responding to that hit. However, raising the number of elements added together also increases the probability that two or more hits will be counted as one. For this reason, it is important to determine the algorithm which best meets the requirements of full energy reconstruction and low multiple-hit probability. In this context a multiple-hit is defined as two or more hits that are treated as a single shower due to the event reconstruction.

The method adopted in this work is to add together the energy from contiguous detectors following the approach of the TAPS group [13]. The γ-ray identification is done by a two dimensional energy versus TOF cut, with the added condition against pielup that the pulse shape of the BaF$_2$ signal should have the proper ratio of fast component to slow light output [11]. Elements are then assigned to a shower where all detectors in a shower are direct neighbors to each other; the energy deposited in these elements is then added together to give the total energy deposited by that hit.

An alternative algorithm is to relax the contiguity condition to allow a gap between detectors that are included in the energy addback. One way to formulate this in software is to determine neighbors based upon the distance between the center of crystals, d, which registered a hit. Strict contiguity would require $d \leq 2r_{det}$, where r_{det} is the inscribed crystal radius. A relaxed contiguity might require $d \leq 4r_{det}$. Figure 2 shows the results of calculations for three γ-ray energies using the Monte Carlo electromagnetic shower simulation code GEANT [14] including the full array and target chamber geometry. It is clear that the more relaxed condition improves the reconstructed peak efficiency. However, due to the hexagonal geometry the number of elements in a cluster increases from 7 to 19 which nearly triples the multiple-hit probability. On the other hand, the cost of the strict contiguity (or nearest-neighbor) condition is the production of "secondary" showers due to the event reconstruction algorithm. As can be seen in the low energy region of Fig. 2, these "secondary" showers generally fall below T_h. For the strongly exponential γ-ray spectra from fusion-fission reactions, such showers are not discernible. Thus, the contiguity condition was selected as the most appropriate event reconstruction algorithm.

Figure 3 illustrates the data reduction process, where different gates are applied to the experimental γ-ray spectra. The high granularity of the array greatly reduces the number of pileup events and so the fast/slow cut has almost no effect. The energy versus time-of-flight gate on the other hand is extremely important in eliminating the fast-neutron background. The difference between summing together all elements in the array or performing a full event reconstruction is very noticeable. This again highlights the importance of a reliable event reconstruction algorithm.

The same event reconstruction procedure was used to build the array response matrix required for comparison of the theoretical spectra to the experimental data. First, GEANT was used to generate events resulting from incident monoenergetic γ-rays with $E_\gamma = 1$ to 25 MeV. The energy deposited in each detector was folded with a Gaussian distribution to account for photon statistics of the initial shower, incomplete light collection of the photomultiplier tubes, and electronic noise. The average energy resolution of the BaF$_2$ detectors
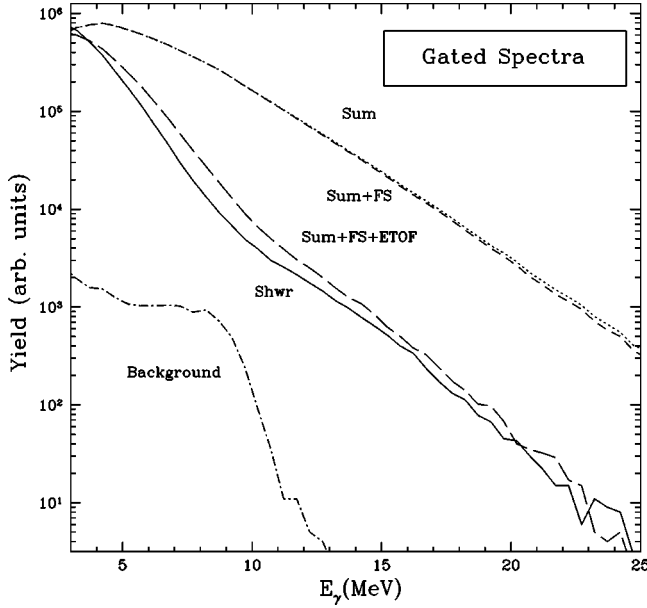
FIG. 3. Experimental γ-ray spectra from 285 MeV ^{32}S$+^{208}$Pb$\rightarrow^{240}$Cf displaying the total array energy summed into one spectrum (dotted), with the fast versus slow cut (FS) applied to reject pileup events (short dashed), and then with FS and the energy versus time-of-flight cut (ETOF) applied to select γ rays (long dashed). The full event (shower) reconstructed spectra (Shwr) are shown as a solid line, while the background is plotted with a dotted-dashed line.

was experimentally determined to be $\sigma(E_\gamma)/E_\gamma = 0.023 + 0.045/E_\gamma^{1/2}$. The T_h and T_l thresholds were then applied in software to match the experimental conditions. Finally, the event reconstruction was performed on these events and the simulated spectrum for a given monoenergetic γ-ray was created. Such simulated spectra are compared to experimental data from both the large BaF$_2$ array and the small 7 element array in Fig. 4. The simulated line shapes are found to be in excellent agreement with the experimental data at all three energies. A response matrix was then built from this series of GEANT simulations.
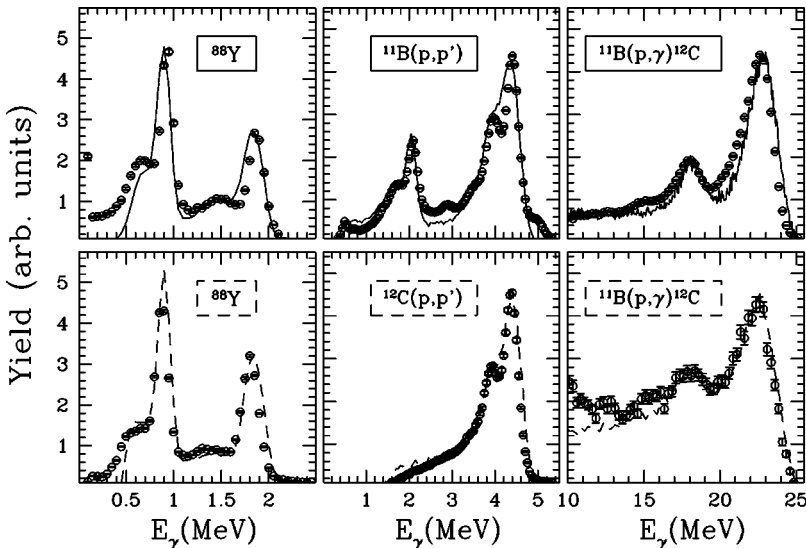
C. Experimental results

Figure 5 presents the absolute γ-ray/fission multiplicities measured at all seven bombarding energies using the large BaF$_2$ array in coincidence with the MWACs. A clear increase in high energy γ-ray yield is apparent from inspection of these data. The experimental spectra also scale smoothly with bombarding energy as expected.

In our analysis the experimental mass distributions were obtained from a full event reconstruction of kinematically coincident fission fragments using the Casini method [15]. This method corrects for in-flight particle emission and angle straggling in the target which alters the measured velocity vectors from their initial values. An iterative energy correction calculation was carried out to compensate for energy loss in the target. With this correction the total kinetic energy (TKE) of the event and individual fragment masses were calculated. The mass distributions peak around the symmetric mass split. Figure 6 shows the extracted standard deviation of the fragment mass distributions compared to the theoretical calculation according to Ref. [16]. Except for the two highest energy data point the mass widths are well described by the calculation.

III. THE MODEL

The analysis of the data was carried out with a modified version of the statistical model code CASCADE [2,17] which includes the effects of nuclear dissipation on the fission width and the saddle to scission time [18–23]. The various model assumptions and the recent improvements to this code have been discussed in Ref. [4]. Only the relevant aspects of nuclear dissipation are surveyed in the present work.

The fission width is calculated according to the saddle point transition state model using the Bohr-Wheeler formula [24]:

$$\Gamma_{\text{fiss}}^{\text{BW}} = \frac{1}{2\pi\rho_1(E_i,J_i)} \int_0^{E_i-E_b} \rho_2(E_i - E_b - E, J_i)dE, \quad (1)$$

FIG. 4. Comparison of experimental data to GEANT generated spectra (lines) for the full BaF$_2$ array (top panels) and the small seven element array (bottom panels).
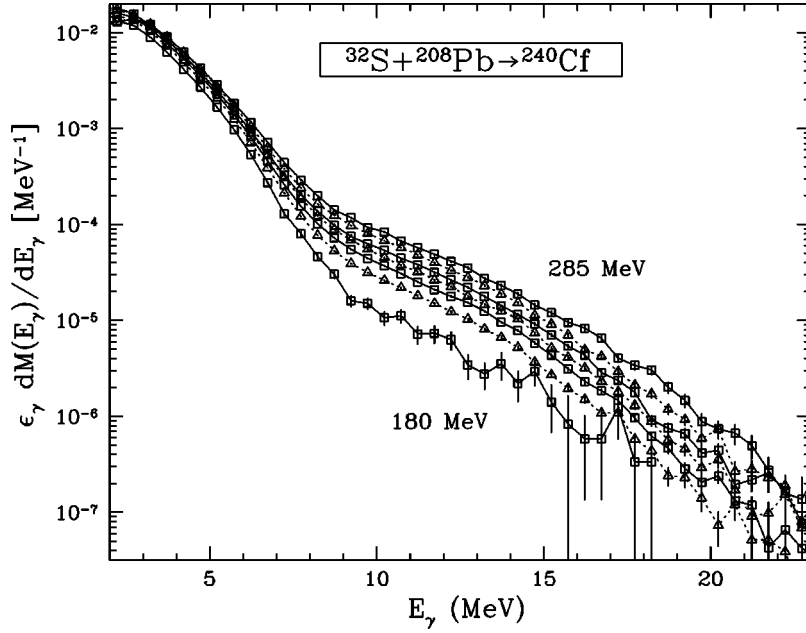
FIG. 5. The experimental absolute γ-ray/fission multiplicities from ^{32}S$+^{208}$Pb$\rightarrow^{240}$Cf for $E_{\text{lab}}=180$ to 285 MeV. The solid and dotted lines are to guide the eye.

where $E_b(J_i)=E_{\text{rot}}(J_i)+E_f(J_i)$; E_{rot} is the rotational energy and $E_f(J_i)$ is the angular momentum dependent fission barrier; ρ_1 is the level density at the initial state (E_i,J_i), whereas ρ_2 is the level density at the saddle point. The fission width is related to the decay rate by $\Gamma_f=\hbar R_{\text{fiss}}$. In the constant temperature approximation (1) reduces to

$$\Gamma_f^{\text{BW}}=\frac{T}{2\pi}\exp(-E_f/T). \qquad (2)$$

The validity of this particular form as a function of excitation energy and spin has been a topic of much discussion [25,26]. However, we emphasize that CASCADE computes the exact integral form of the fission width and the simplified form in Eq. (2) is not used.

Nuclear dissipation affects the fission process in three ways. The first is a reduction of the fission width as shown by Kramers [27], where

$$\Gamma_f^{\text{Kramers}}=\Gamma_f^{\text{BW}}[(1+\gamma^2)^{1/2}-\gamma] \qquad (3)$$

is the dissipative fission width. Here the nuclear dissipation parameter γ determines the extent of the reduction and is

related to the reduced dissipation coefficient β by $\gamma=\beta/2\omega_0$ [19,22] where ω_0 describes the curvature of the potential energy surface at the saddle point (the barrier frequency). The second effect is a buildup time required for the fission width to reach its quasistationary value:

$$\Gamma_f(t)=\Gamma_f^{\text{Kramers}}[1-\exp(-2.3t/\tau_f)], \qquad (4)$$

where τ_f is the delay time for the fission flux to reach 90% of the quasistationary value. Semiquantitative analytical expressions for the transient time τ_f are given in Refs. [22,23]. For overdamped motion $\tau_f=(\beta/2\omega_1^2)\ln(10E_f/T)$ where ω_1 is the assault frequency inside the barrier, E_f is again the fission barrier height, and T is the nuclear temperature. The third effect is an increase of the saddle to scission time

$$\tau_{\text{ssc}}=\tau_{\text{ssc}}^0[(1+\gamma^2)^{1/2}+\gamma], \qquad (5)$$

where τ_{ssc}^0 is the nondissipative saddle to scission time [28].

The fission barrier in a highly fissile, hot system becomes smaller than the temperature T at a relatively low angular momentum and the fission process is completely governed by transients. It was shown by Weidenmüller and Jing-Shang
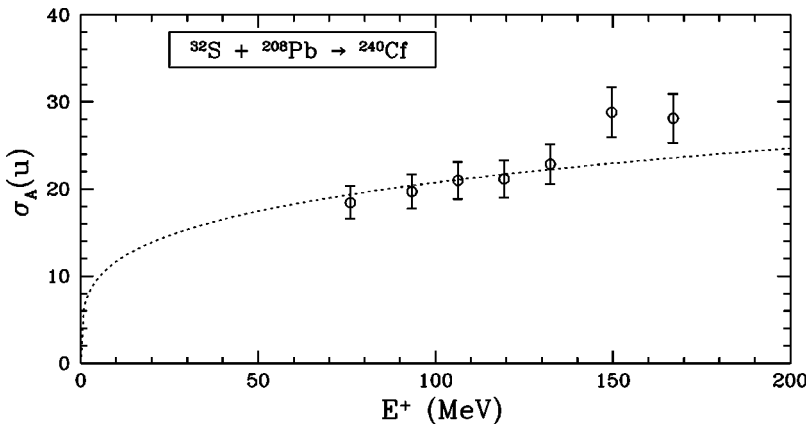
FIG. 6. Measured standard deviation of the fragment mass distributions from ^{240}Cf compared to a calculation based on Ref. [16].
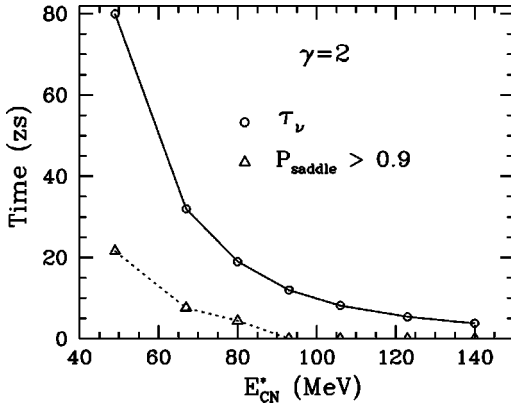
FIG. 7. Calculated average neutron lifetime (circles) for ^{240}Cf and time at which the probability of finding the system to the right of the saddle point (P_{saddle}) exceeds 90% (triangles) (based upon Ref. [20]).

[20] and further discussed by Grangé [21] that in this case the stationary probability flow over the barrier may never be reached. Then the Kramers formula, Eq. (3), is not applicable and the buildup time constant τ_f characterizes the pre-saddle lifetime. In Fig. 7 we show for ^{240}Cf the calculated average neutron lifetime and the time at which 90% of the fission flux has passed the saddle point (based upon Fig. 3 of Weidenmüller and Jing-Shang [20]) as a function of the CN excitation energy, E^*_{CN}. This figure demonstrates that in the present system the saddle point is already passed before any significant presaddle neutron emission can occur. Other decay channels have even longer time scales than neutron emission.

This temperature dependent dynamical effect as implemented in our extended CASCADE code was referred to as the ''fast fission'' process in our previous work [4]. We emphasize that though the term fast fission has traditionally been used in literature [29] for processes where a compact system is formed and decays promptly without any fission barrier, the transient process that we describe here drives the system quickly to the scission even with a small nonzero barrier.

In our calculations we modeled this fast transient fission process in the following simplified manner. When the ratio of the fission barrier and nuclear temperature are less than a predetermined input parameter (e.g., $E_f/T < k$), particle and γ-ray decay are not allowed. Instead, the corresponding population is transferred to the saddle point and will undergo only the saddle to scission decay. According to Weidenmüller and Jing-Shang [20] the transients become dominant for $k \approx 0.5$. The nuclear viscosity still plays a role by affecting the saddle to scission motion [see Eq. (5)].

It is known from fission fragment angular distribution measurements that quasifission plays an important role in the ^{32}S+^{208}Pb reaction [10]. To overcome the unconditional fusion barrier an extra-extra push energy E_{xx} is required. The extra-extra push energy is angular momentum dependent, and above a critical angular momentum the CN is not formed in our reaction. The mass exchange process between the projectile and the target is incomplete, the neck is preserved, and the movement towards the scission point starts before
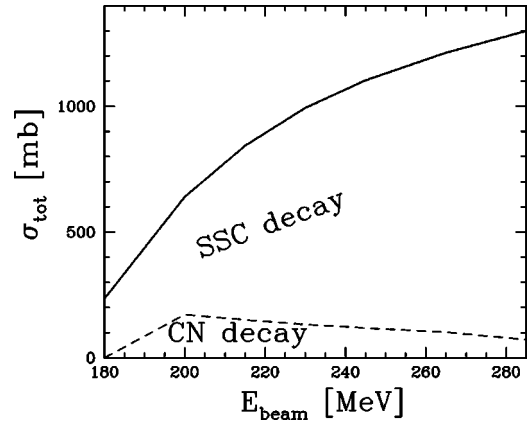
FIG. 8. Contribution of the different decay types. The total cross section σ_{tot}, which is the sum of the complete fusion and quasifission cross section is plotted as a function of bombarding energy. The area marked ''CN decay'' corresponds to that part of the cross section, which will decay inside the saddle point, whereas most of the cross section decays only during the saddle to scission decay (''SSC decay'').

the full equilibrium has been reached. Extra-push model calculations, based on the model of Shen *et al.* [16] yield 100% quasifission at 180 MeV bombarding energy decreasing to 50–60 % for the higher beam energies.

Figure 8 pictures the contribution of possible decay types involved in the present experiment. Presaddle decay takes place only up to $\approx$ 170 mb cross section, whereas most of the cross section decays during the saddle to scission motion.

Since in hot ^{240}Cf the decay is dominated by the saddle to scission decay process, an accurate calculation of τ^0_{ssc} is important for extraction of the nuclear viscosity parameter from Eq. (5). The value of τ^0_{ssc} for ^{240}Cf can be estimated from the work of Nix [30] to be $\approx$4 zs(1 zs=1×10^{-21} s). A more quantitative approach calculates τ^0_{ssc} using the analytical expression [22,28]

$$\tau^0_{ssc} = \frac{2}{\omega_0} R[(\Delta V/T)^{1/2}], \qquad (6)$$

where

$$R(z) = \int_0^z \exp(y^2) dy \int_y^\infty \exp(-x^2) dx. \qquad (7)$$

Here ΔV is the potential energy difference between the saddle point and the scission point, T is the nuclear temperature, and ω_0 is again the barrier frequency. Table II presents the quantities involved in a calculation of the nondissipative saddle to scission time for ^{240}Cf assuming a spin independent barrier frequency, $\omega_0 = 1$ zs^{-1}. These calculations give a nondissipative saddle to scission time of $\tau^0_{ssc} \approx 2.7$ zs. We note that the trend indicated in the barrier frequency calculations of Ref. [31] suggest that ω_0 decreases slightly with increasing angular momentum.

An issue which has yet to be resolved in the literature is the proper handling of the excitation energy of the system during the descent from saddle to scission [2,32–35]. This

TABLE II. Calculation of τ^0_{ssc} for ^{240}Cf. The columns list the beam energy (E_{lab}) and the corresponding average angular momentum (l_{ave}) and initial temperature (T) assuming $E^* = aT^2$ with $a = A/9$, the potential energy difference between the saddle point and the scission point (ΔV), $R[(\Delta V/T)^{1/2}]$, and the nondissipative saddle to scission time τ^0_{ssc} calculated from Eq. (6) assuming $\omega_0 = 1$ zs^{-1}. The potential energy surface was calculated according to the method of Ref. [31].

E_{lab} (MeV)	l_{ave} ($\hbar$)	T (MeV)	ΔV (MeV)	$R[(\Delta V/T)^{1/2}]$	τ^0_{ssc} (zs)
180	20.8	1.31	44.0	1.38	2.76
230	61.3	1.84	51.3	1.32	2.64
285	78.1	2.27	57.4	1.24	2.58

becomes of paramount importance for systems in which the prescission particle and γ-ray spectra are dominated by saddle to scission emission. The method used in previous GDR γ-ray studies (e.g., Ref. [2]) adds an offset energy ΔE_x to the system at the beginning of the saddle to scission calculation so that $E_{ssc*} = E_{CN*} + \Delta E_x$. This offset energy may be positive or negative depending upon the mass of the system [32]. It corrects in an average way for the change in the potential energy between the saddle and scission points. An alternative method was used in investigations of neutron emission from fusion-fission and quasifission system by Hinde et al. [32]. They treat the offset energy ΔE_x as a free parameter and add this energy to the initial excitation energy of the system.

In the present investigation we implemented a more transparent method to calculate the (angular momentum dependent) saddle to scission offset energy directly from the potential energy surface. Here the energy offset is determined as the difference between the potential energy at the equilibrium position and a position between the saddle and scission points. The parameter d determines this position as the fraction of the total deformation change between the saddle and scission points. The potential energy surface was calculated using the method of Lestone [31].

The $J = 0$ $\hbar$ potential energy surface for ^{240}Cf is shown in the top panel of Fig. 9 to illustrate the saddle to scission offset energy calculation. The calculated offset energies are shown in the bottom panel as a function of angular momentum for three values of the parameter d where $d = 0$ corresponds to the saddle point and $d = 1$ to the scission point. The values of ΔE_x extracted from the experimental neutron data from two $A_{CN} = 239$ systems [32] are also plotted at the mean values of the corresponding fusion angular momentum distributions. The angular momentum dependent offset energies were included as an option in CASCADE and used for the calculations presented in this work. In the present investigation we selected a value of $d = 0.5$ for determining the offset energy.

The level density prescription used in the present work is taken from Ignatyuk et al. [36] who proposed a form which reflects the nuclear shell structure at low excitation energy and goes smoothly to the liquid drop behavior at high excitation energy. Here the level density parameter is taken as a

smooth function of mass but with an energy-dependent factor which introduces the shell structure explicitly:

$$a(U) = \tilde{a}\left(1 + \frac{f(U)}{U} \delta W\right),$$

$$f(U) = 1 - \exp(-U/E_D),$$

(8)

where U is the thermal energy of the system, $\tilde{a}$ is the asymptotic (or liquid drop) level density parameter, E_D determines the rate at which the shell effects melt away, and δW is the shell correction taken from the difference between the experimental and liquid drop model (LDM) masses ($\delta W = M_{exp} - M_{LDM}$). Reisdorf [37] determined a formula for the asymptotic level density parameter reminiscent of liquid drop mass calculations:

$$\tilde{a} = 0.04543 r_0^3 A + 0.1355 r_0^2 A^{2/3} B_S + 0.1426 r_0 A^{1/3} B_K, \quad (9)$$

where A is the nuclear mass, r_0 is the nuclear radius, and B_s and B_k are the surface and curvature terms of the liquid drop model, respectively. The pairing energy is given as $\Delta = \chi(p/A^{1/2})$ where $\chi = +1, -1, 0$ for even-even, odd-odd, and odd nuclei, respectively. A fit to the available s-wave resonance neutron spacings resulted in the values $r_0 = 1.153 \pm 0.01$ fm, $p = 10.5 \pm 2$ MeV and $E_D = 18.5$ MeV [37]. In the present work the shape dependences, B_s and B_k, are deter-
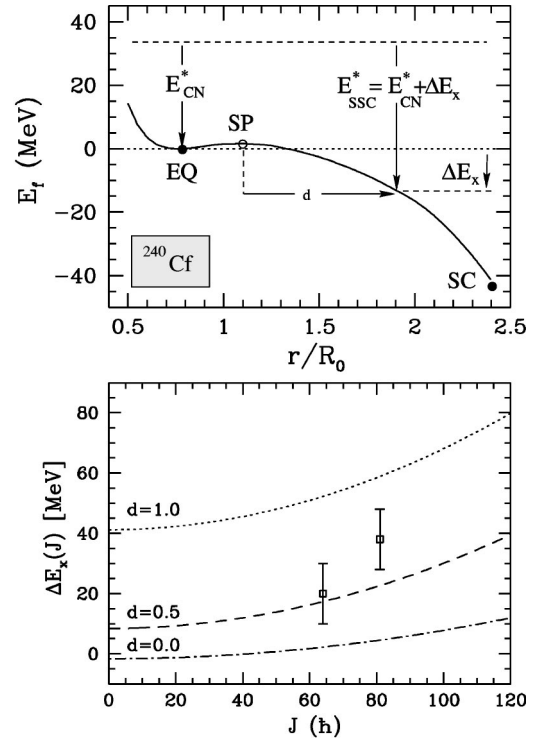
FIG. 9. Top panel: potential energy surface for $J = 0\hbar$ ^{240}Cf calculated using Lestone's method [31]. Circles indicate the equilibrium, saddle, and scission points, respectively. Bottom panel: calculated saddle to scission offset energy (see text) for three values of the parameter d. The data points are the offset energies extracted from 249 MeV ^{40}Ar + ^{197}Au and 418 MeV ^{64}Ni + ^{175}Lu in Ref. [32]. The top panel is adapted from Hinde et al. [32].
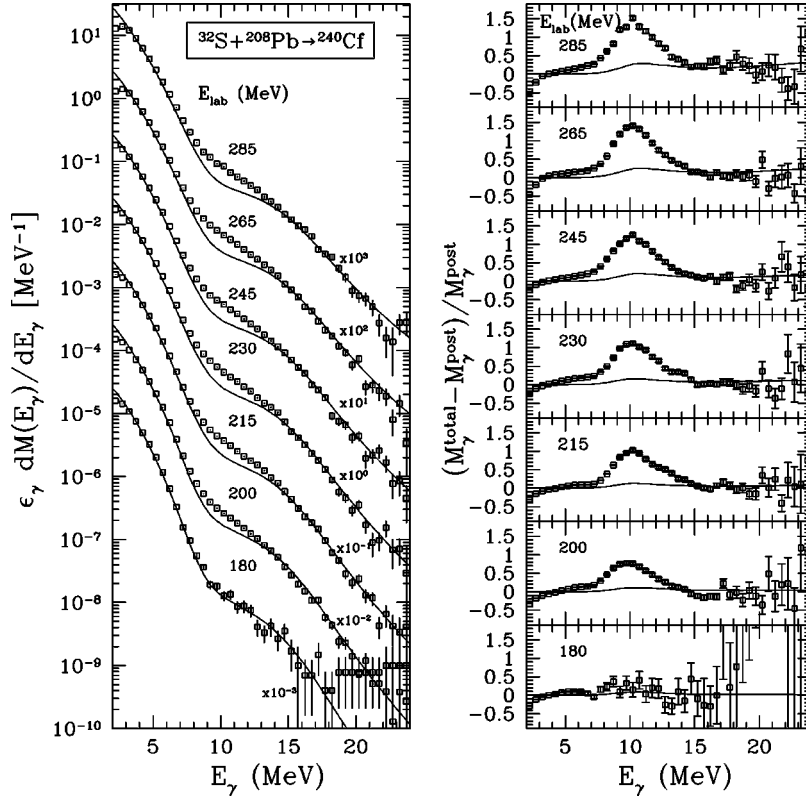
FIG. 10. ^{32}S+^{208}Pb→^{240}Cf absolute γ-ray/fission multiplicities for $E_{lab}=180$ to 285 MeV compared to a series of calculations which do not include dissipation. The left panel presents the data and calculations on the absolute scale. The right panel provides a display in the more sensitive divided representation (see text). The calculations have been folded with the BaF$_2$ array response matrix.

mined from the nuclear deformation [38] which is an input variable in the calculation. The shape dependences are $B_s = B_k = 1$ for a spherical nucleus.

Our previous study of ^{224}Th found that an additional temperature dependence in the level density prescription was required to fit the high energy γ-ray spectra [4]. The final form of the level density parameter is then

$$a(T) = a(U)[1 - \kappa f(T)],$$
$$f(T) = 1 - \exp[-(TA^{1/3}/21)^2], \quad (10)$$

where $a(U)$ is calculated according to Eq. (8) and k determines the strength of the additional temperature dependence. This function is drawn from expressions for the temperature dependence of the mean-field parameters in Ref. [39].

IV. ANALYSIS

Figure 10 compares the absolute experimental γ-ray/fission multiplicities compared to a series of calculations without dissipative effects. The experimental and theoretical spectra are presented on both an absolute scale without any normalization and also using the more sensitive "divided" representation introduced in Ref. [4]. Here the difference between the total spectrum and the calculated post-scission (i.e., fission fragment) spectrum is divided by the calculated post-scission spectrum. This representation is model dependent but provides a sensitive scale which reveals even minor differences between the data and the theoretical calculations which are otherwise not apparent from the strongly exponential spectra.

The theoretical calculations shown in Fig. 10 were performed using the Ignatyuk/Reisdorf nuclear level density formalism [36,37]. The nuclear radius parameter r_0 was taken as 1.153 for the CN and $r_{0,f} = 1.10$ for the fission fragments. No additional temperature dependence was included in the level density prescription for these calculations (i.e., $\kappa = 0$). The full Sierk fission barriers [40] for this system were used without any scaling. The average saddle to scission quadrupole deformation of $\beta = 0.6$ was taken from the liquid drop model [41]. The GDR parameters determined in the final analysis below were calculated assuming a prolate shape of smaller deformation $\beta = 0.3$. Since the majority of high energy GDR γ-rays are emitted during the first few decay steps, the shape of the CN GDR will reflect the smaller initial deformation. The CN and saddle to scission (SSC) GDR parameters are listed in Table III.

For most of the calculations it was assumed that the GDR exhausts 100% of the classical sum rule (SR), based on the systematics given by Gaardhøje [42] and on the observation that the observed ground-state GDR yield up to 25 MeV (the present fitting range) yields 1 SR. It has been pointed out

TABLE III. GDR parameters for ^{32}S+^{208}Pb→^{240}Cf. A positive (negative) deformation parameter indicates a prolate (noncollective oblate) deformation. The GDR centroid is 12.7 MeV for both the CN and SSC decay.

System	β	E_1 (MeV)	Γ_1 (MeV)	E_2 (MeV)	Γ_2 (MeV)
CN	-0.1	12.3	4.5	13.5	5.3
SSC	$+0.3$	10.7	4.0	13.7	6.4
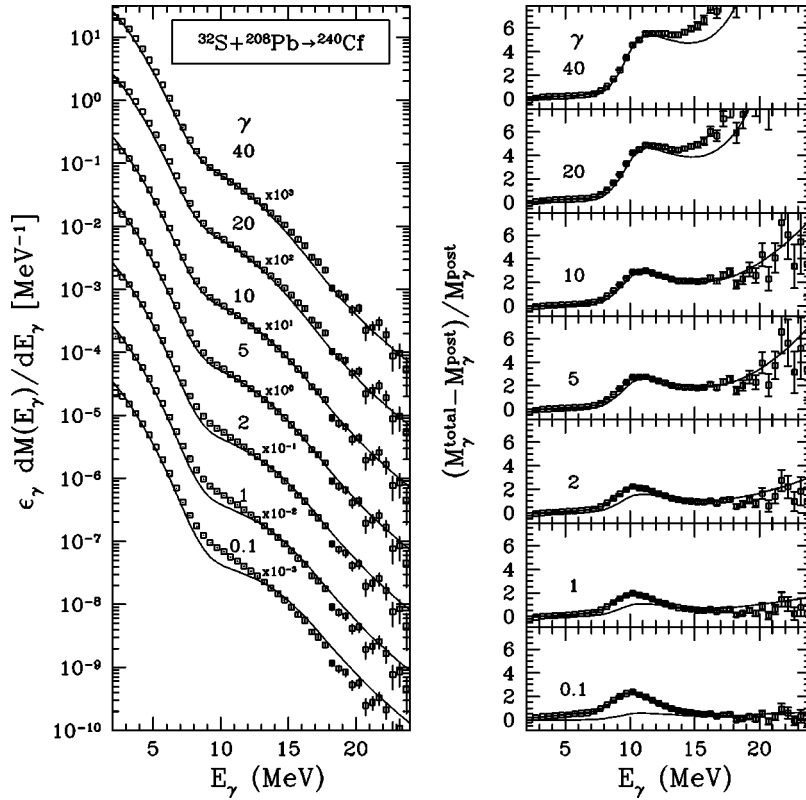
FIG. 11. Various fits for the 245 MeV data. The viscosity outside the saddle (γ_o) is varied between 0.1 and 40. Temperature dependence of level densities ($\kappa=0.4$) is also included.

recently [43] that in very heavy nuclei a single-Lorentzian fit of the ground-state GDR up to the π-threshold exhausts about 1.1–1.3 SR [44]. The additional strength is well understood being due to exchange effects that occur at higher energies. Calculations using both strengths have been investigated with the following conclusion. The strength under a single-Lorentzian fit scales as

$$(\pi/2)\sigma_m\Gamma = x \times 60NZ/A, \qquad (11)$$

where σ_m is the maximum measured cross section and x is the ratio of the experimental to the classical SR. Since Γ/x $=$const, a GDR width obtained from fitting a limited region of observation compensates for the SR enhancement x. Thus we favor the use of $x=1$ (i.e., 100% SR) in the fitting procedures used in this paper.

The fission fragment GDR decay was assumed to exhaust 100% of the classical sum rule, to have a width of 6.5 MeV and a single component GDR centroid energy according to the systematics of Ref. [42]. The saddle to scission offset energy ΔE_x was determined for the position halfway between saddle and scission (i.e., $d=0.5$).

The measured absolute γ-ray/fission multiplicities shown in Fig. 9 agree well with the calculations for $E_\gamma < 7$ MeV and $E_\gamma > 14$ MeV for all seven bombarding energies. At these energies the γ-rays originate almost entirely from the fission fragments. However, except for the lowest bombarding energy, a significant excess γ-ray yield can be seen in precisely the CN GDR region from $E_\gamma=7$ to 14 MeV. This excess cannot be explained within a purely statistical decay analysis but rather a nuclear dissipative mechanism has to be invoked. We also note that the observed enhancement due to

nonzero viscosity is much larger than can be obtained from any reasonable SR enhancement.

Several series of calculations were performed including nuclear dissipation as described in the Model section. Since the overwhelming amount of γ-rays is emitted during the saddle to scission motion, the calculations are rather insensitive to the value of the dissipation inside the saddle (γ_i). Increasing the value of the dissipation during the saddle to scission motion (γ_o) increases the saddle to scission time according to Eq. (5), and thus an increase in the saddle to scission γ-ray emission is observed in the 10 MeV energy region. At the same time the system will arrive to the scission point at lower temperature, yielding colder fission fragment production, which results in a decrease in the high energy γ-ray emission and the calculations underpredict the high energy tail of the spectra. The lower yields of γ-rays in the calculated high energy tail conforms with the trends observed in our previous analysis of γ-rays from ^{16}O$+^{208}$Pb $\rightarrow^{224}$Tb [4]. In that analysis the high energy tail was fitted by including an additional temperature dependence in the level density prescription [see Eq. (10)] where $\kappa=0.8$ was required to fit the γ-ray spectra. In the present reaction we found weaker temperature dependence $\kappa=0.4$.

As an illustration of the fitting procedure on Fig. 11 we present a series of calculations for the 245 MeV beam energy data. The γ-ray yield at about 10 MeV gradually increases with the viscosity parameter γ. We obtained a good fit for $\gamma=5$ to 10, whereas for higher γ-s the fit starts to underpredict the high energy tail.

Similar calculations were performed for each bombarding energy. It was found that we need $\gamma_o=5$ or higher to fit the data, and for $\gamma_o \geqslant 20$ the high energy tail was underpredicted.
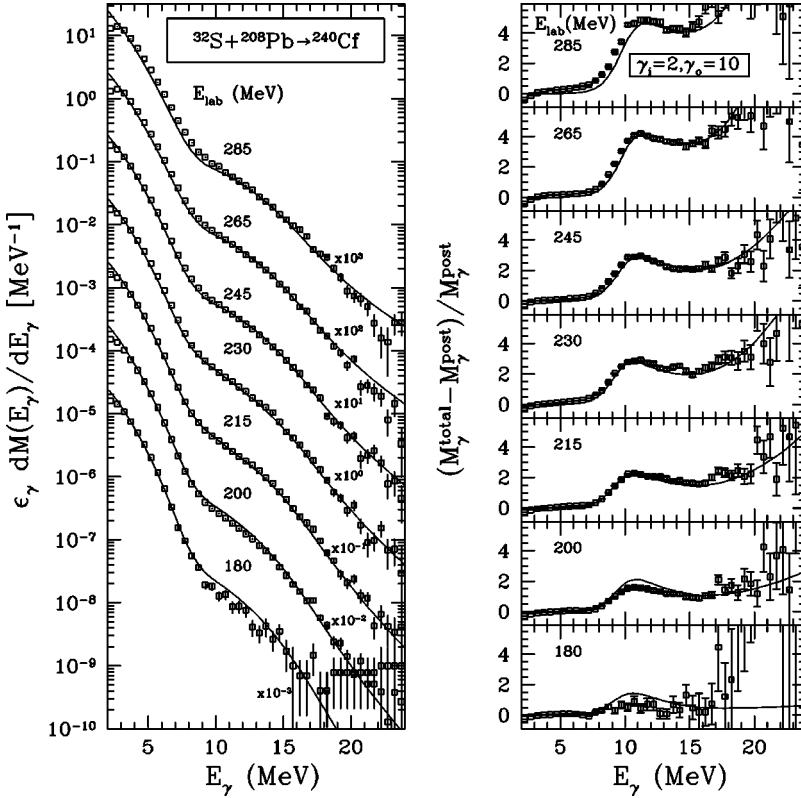
FIG. 12. Same as Fig. 10 but with $\gamma_i = 2$, $\gamma_o = 10$, and temperature dependent level densities according to Eq. (10) with $\kappa = 0.4$.

Figure 12 shows the $\gamma_o = 10$ fit for each bombarding energy. The quality of the fits is good except for a slight overprediction in the 10 MeV region for the lowest two bombarding energies. We note, however, that at the lowest excitation energies our method is less sensitive: there is too little excess over the fission fragment γ-rays to determine the viscosity value. The good fits with constant viscosity rule out the use of a temperature dependent nuclear viscosity parameter for the saddle to scission decay.

V. DISCUSSION

Statistical model calculations without the inclusion of dissipation were found to under-predict the γ-ray/fission multiplicities in the GDR region around $E_\gamma = 10$ MeV for all but the lowest bombarding energy. When nuclear dissipation was included the high energy γ-ray tail was underpredicted necessitating an additional level density temperature dependence. The magnitude of this additional temperature dependence was somewhat smaller than that used for the previous analysis of excited ^{224}Th.

There are important differences between ^{240}Cf and ^{224}Th. The fission barrier for ^{240}Cf is only 1.6 MeV at $J = 0\hbar$ compared to 5.7 MeV for ^{224}Th. Furthermore in the ^{32}S $+$ ^{208}Pb reaction there is a considerable contribution of quasifission cross section. Therefore the particle and γ-ray decay inside the saddle has only a small contribution, the measured γ-rays originate from the saddle to scission motion. The measured nuclear viscosity in ^{240}Cf characterizes the viscosity of the saddle to scission motion.

A deformation dependent nuclear dissipation, modeled here by a small constant dissipation $\gamma_i = 2$ inside the saddle

and a larger constant dissipation $\gamma_o = 10$ outside the saddle, combined with a temperature dependent level density prescription provided the best fit to the data. The lowest energy data point requires lower viscosity, in agreement with the previous observation [6]. However, according to the extra push calculations the quasifission contribution is highest at the low bombarding energies, therefore the excitation energy could in reality be lower than that assumed in our calculations, which would result in lower γ-ray yield with the same viscosity. We also note that at the lowest beam energies the excitation energy of the system is very low, and the method to extract a viscosity from the measured γ-ray yield becomes less reliable.

The proposed method for determining the saddle to scission energy (discussed in Sec. III) highlights a large uncertainty in calculations involving fusion-fission systems where saddle to scission emission dominates the pre-scission particle and γ-ray spectra. In the current model, the saddle to scission offset energy was obtained from the potential energy change halfway between saddle and scission. The saddle to scission time obtained with this method ($\tau_{ssc} \approx 54$) is slightly longer than the result of Ref. [32] which obtained a dynamical time scale of $\tau = 35$ zs.

It is important to note that the choice of level density prescription also affects the magnitude of the saddle to scission time, and consequently the derived viscosity parameter. In the ^{16}O $+$ ^{208}Pb $\rightarrow$ ^{224}Th analysis of Ref. [4], introducing the additional temperature dependence of Eq. (10) reduced the maximum required value of the viscosity parameter from $\gamma = 14$ to $\gamma = 8$. The earlier investigation of ^{240}Cf in Ref. [8] also showed that changing the level density parameter from

$a=A/8$ to $A/10$ reduced the extracted saddle to scission time from $\tau_{ssc}=34$ zs to 15 zs.

It is clear that these significant model uncertainties in the saddle to scission offset energy and the level density prescription preclude a precise determination of the saddle to scission time and therefore the viscosity parameter from the present analysis. However, the trends observed here for nuclear dissipation in ^{240}Cf are independent of these systematic uncertainties. Thus the present measurement over an extended temperature range indicate that a temperature dependent dissipation is not warranted for ^{240}Cf within the statistical model including dissipation. This temperature independent behavior combined with the large value of γ points strongly to a one-body mechanism for nuclear dissipation. This conclusion thus favors the choice of one-body dissipation for the case of ^{224}Th as well.

[1] M. Thoennessen, D. R. Chakrabarty, M. G. Herman, R. Butsch, and P. Paul, Phys. Rev. Lett. **59**, 2860 (1987).

[2] R. Butsch, D. J. Hofman, C. P. Montoya, P. Paul, and M. Thoennessen, Phys. Rev. C **44**, 1515 (1991).

[3] I. Diószegi, D. J. Hofman, C. P. Montoya, S. Schadmand, and P. Paul, Phys. Rev. C **46**, 627 (1992).

[4] I. Diószegi, N. P. Shaw, I. Mazumdar, A. Hatzikoutelis, and P. Paul, Phys. Rev. C **61**, 024613 (2000).

[5] H. Rossner, D. J. Hinde, J. R. Leigh, J. P. Lestone, J. O. Newton, J. X. Wei, and S. Elfström, Phys. Rev. C **45**, 719 (1992).

[6] D. J. Hofman, B. B. Back, and P. Paul, Phys. Rev. C **51**, 2597 (1995).

[7] P. Fröbrich and I. I. Gontchar, Phys. Rep. **292**, 131 (1998).

[8] D. J. Hofman, B. B. Back, I. Diószegi, C. P. Montoya, S. Schadmand, R. Varma, and P. Paul, Phys. Rev. Lett. **72**, 470 (1994).

[9] C. R. Morton, A. Buda, P. Paul, N. P. Shaw, J. R. Beene, N. Gan, M. L. Halbert, D. W. Stracener, R. L. Varner, M. Thoennessen, P. Thirolf, and I. Diószegi, J. Phys. G **23**, 1383 (1997).

[10] B. B. Back, R. R. Betts, J. E. Gindler, B. D. Wilkins, S. Saini, M. B. Tsang, C. K. Gelbke, W. G. Lynch, M. A. McMahan, and P. A. Baisden, Phys. Rev. C **32**, 195 (1985).

[11] W. J. Kernan, N. Gan, A. L. Caraley, B. J. Fineman, R. L. McGrath, and R. J. Vojtech, Nucl. Instrum. Methods Phys. Res. A **313**, 563 (1992).

[12] N. P. Shaw, Ph.D. thesis, Stony Brook, 1999.

[13] A. R. Gabler et al., Nucl. Instrum. Methods Phys. Res. A **346**, 168 (1994).

[14] R. Brun et al., GEANT3, CERN-DD/EE/84-1 (1986).

[15] G. Casini, P. R. Maurenzig, A. Olmi, and A. A. Stefanini, Nucl. Instrum. Methods Phys. Res. A **277**, 445 (1989).

[16] W. Q. Shen et al., Phys. Rev. C **36**, 115 (1987).

[17] F. Pühlhofer, Nucl. Phys. **A280**, 267 (1977).

[18] P. Grangé and H. A. Weidenmüller, Phys. Lett. **96B**, 26 (1980).

[19] P. Grangé, Li Jun-Qing, and H. A. Weidenmüller, Phys. Rev. C **27**, 2063 (1983).

[20] H. A. Weidenmüller and Zhang Jing-Shang, Phys. Rev. C **29**, 879 (1984).

[21] P. Grangé, Nucl. Phys. **A428**, 37c (1984).

[22] P. Grangé, S. Hassani, H. A. Weidenmüller, A. Gavron, J. R. Nix, and A. J. Sierk, Phys. Rev. C **34**, 209 (1986).

[23] K. H. Bhatt, P. Grangé, and B. Hiller, Phys. Rev. C **33**, 954 (1986).

[24] N. Bohr and J. A. Wheeler, Phys. Rev. **56**, 426 (1939).

[25] M. Thoennessen, Nucl. Phys. **A599**, 1 (1996).

[26] J. P. Lestone, Phys. Rev. C **59**, 1540 (1999).

[27] H. A. Kramers, Physica (Amsterdam) **7**, 284 (1940).

[28] H. Hofmann and J. R. Nix, Phys. Lett. **122B**, 117 (1983).

[29] C. Ngô, Prog. Part. Nucl. Phys. **16**, 139 (1986).

[30] J. R. Nix, Nucl. Phys. **A130**, 241 (1969).

[31] J. P. Lestone, Phys. Rev. C **51**, 580 (1995).

[32] D. J. Hinde, D. Hilscher, H. Rossner, B. Gebauer, M. Lehmann, and M. Wilpert, Phys. Rev. C **45**, 1229 (1992).

[33] D. Hilscher and H. Rossner, Ann. Phys. (Paris) **17**, 471 (1992).

[34] J. Wilczyński, K. Siwek-Wilczyńska, and H. W. Wilschut, Phys. Rev. C **54**, 325 (1996).

[35] J. Velkovska, C. R. Morton, R. L. McGrath, P. Chung, and I. Diószegi, Phys. Rev. C **59**, 1506 (1999).

[36] A. V. Ignatyuk, G. N. Smirenkin, and A. S. Tishin, Yad. Fiz. **21**, 485 (1975) [Sov. J. Nucl. Phys. **21**, 255 (1975)].

[37] W. Reisdorf, Z. Phys. A **300**, 227 (1981).

[38] R. W. Hasse, Ann. Phys. (N.Y.) **68**, 377 (1971).

[39] S. Shlomo and J. B. Natowitz, Phys. Rev. C **44**, 2878 (1991).

[40] A. J. Sierk, Phys. Rev. C **33**, 2039 (1986).

[41] M. Bolsterli, E. O. Fiset, J. R. Nix, and J. L. Norton, Phys. Rev. C **5**, 1050 (1972).

[42] J. J. Gaardhøje, Annu. Rev. Nucl. Part. Sci. **42**, 483 (1992).

[43] M. P. Kelly, K. A. Snover, J. P. S. van Schagen, M. Kicińska-Habior, and Z. Trznadel, Phys. Rev. Lett. **82**, 3404 (1999).

[44] B. L. Berman and S. C. Fultz, Rev. Mod. Phys. **47**, 713 (1975).